ACS Catalysis

Research Article

pubs.acs.org/acscatalysis

Molecular Dynamics Kinetic Study on the Zeolite-Catalyzed Benzene Methylation in ZSM-5

Samuel L. C. Moors,‡ Kristof De Wispelaere,‡ Jeroen Van der Mynsbrugge, Michel Waroquier, and Veronique Van Speybroeck*

Center for Molecular Modeling (CMM), Ghent University, Technologiepark 903, B-9052 Zwijnaarde, Belgium; QCMM-alliance, Ghent-Brussels, Belgium

Supporting Information

ABSTRACT: The methylation of arenes is a key step in the production of hydrocarbons from methanol over acidic zeolites. We performed ab initio static and molecular dynamics free energy simulations of benzene methylation in H-ZSM-5 to determine the factors that influence the reaction kinetics. Special emphasis is given to the effect of the surrounding methanol molecules on the methylation kinetics. It is found that for higher methanol loadings, methylation may also occur from a protonated methanol cluster, indicating that the exact location of the Brønsted acid site is not essential for the zeolite-catalyzed methylation reaction. However, methylations from a protonated methanol cluster exhibit higher free energy barriers than a methylation from a single methanol molecule. Finally, comparison with a pure methanol solvent reaction environment indicates that the main role of the zeolite during the methylation of benzene is to provide the acidic proton and to create a polar environment for the reaction. The metadynamics approach, which is specifically designed to sample rare events, allows exploring new reaction pathways, which take into account the flexibility of the framework and additional guest molecules in the pores and channels of the zeolite framework. This approach goes beyond the often applied static calculations to determine reaction kinetics.

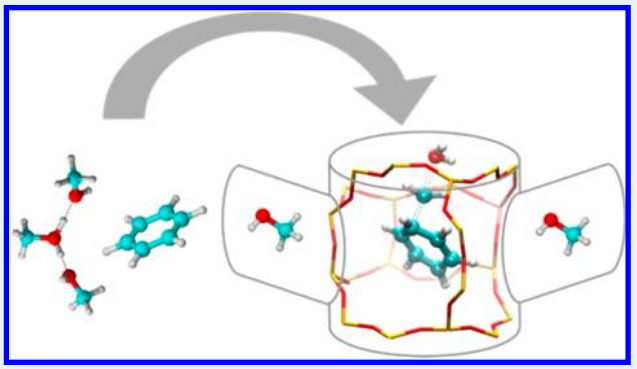

KEYWORDS: *methanol to olefins, ZSM-5, methylation, benzene, methanol clusters, metadynamics*

1. INTRODUCTION

Zeolite-catalyzed processes are ubiquitous in the petrochemical industry nowadays. Among these, the methanol-to-olefin (MTO) conversion over acidic zeolites is one of the most investigated, as its mechanism has proven extremely difficult to unravel.[1−4] The MTO process is an attractive alternative to supply the world with fuels and chemicals starting from nonconventional resources, such as natural gas, coal, or biomass. The archetypal MTO catalysts[5] are H-ZSM-5 and H-SAPO-34 in which Brønsted acid sites are created by isomorphous substitution of heteroatoms. The CHA-structured silicoaluminophosphate H-SAPO-34 shows a high selectivity toward light olefins, whereas the product spectrum for the MFI-structured H-ZSM-5 varies from branched hydrocarbons and aromatics to light olefins, depending on the reaction conditions.[1,5]

The MTO reaction mechanism has been strongly debated, but the hydrocarbon pool (HP) mechanism is now generally accepted.[6−8] The HP consists of organic molecules, both aliphatics and methylated aromatics, occluded in the cages of the inorganic zeolite framework. These species act as essential cocatalysts as they react with the methanol flow; form intermediates; and finally, split off olefins through a closed cycle (paring and side-chain routes).[6−13] The characteristics of the active HP compounds depend on the catalyst topology and process conditions.[1,3] Moreover, for H-ZSM-5, a dual cycle concept has been proposed [13] in which ethene formation through the aromatic-based catalytic cycles is mechanistically separated from the formation of higher alkenes through an autocatalytic cycle with the alkenes as cocatalysts.

During hydrocarbon transformation processes, zeolite-catalyzed alkylation reactions are known to be important reactions.[14] Moreover, in all proposed mechanisms for the MTO process, methylation reactions of the HP species are found to be crucial steps.[15−22] A compilation of the present knowledge on the reaction mechanism of zeolite catalyzed methylation reactions is given by Svelle et al.[23,24] Several mechanisms have been proposed so far. Notably, a distinction is made between a stepwise and a concerted mechanism. In the stepwise mechanism, methanol is dissociated into a surface-bound methoxide and a water molecule prior to the actual methylation. The concerted mechanism, on the other hand, starts from methanol physisorbed at the Brønsted site, and methylation and water elimination occur in a single step.[23] Both mechanisms are schematically displayed in Scheme S1 (Supporting Information).

Received: August 20, 2013
Revised: September 23, 2013

   dx.doi.org/10.1021/cs400706e | ACS Catal. 2013, 3, 2556−2567

Theoretical studies have proven indispensable in unraveling the complex reaction mechanisms governing the MTO process. Initially, various calculations on small zeolite clusters were performed that did not account for the zeolite topology.[25,26] These studies were valuable in their time frame, but currently, it has been shown that topology needs to be taken into account.[16] This is particularly true for bulky aromatic hydrocarbon pool species. Topology may be accounted for by using extended cluster models using a multilevel ONIOM method or by using periodic calculations that take into account the full periodic nature of the catalyst. Some of the present authors proved that with multilevel ONIOM calculations, experimental rates of ethene and propene methylation can be accurately reproduced.[27] Svelle and co-workers showed, using a multistep approach relying on a series of MP2 energy calculations on a variety of clusters and on periodic DFT calculations, that enthalpy barriers for zeolite catalyzed reactions could be calculated with near chemical accuracy.[28] Both papers show that theoretical methods have now matured to a level that calculated energy barriers and reaction rates are directly comparable with experimental data.

The methylation of benzene on H-ZSM-5 and H-Beta has recently been studied both theoretically and experimentally by Van der Mynsbrugge et al.[29] The zeolite catalysts were represented by large cluster models. Geometry optimizations using a two-level ONIOM method were combined with energy refinements at the ωB97X-D level of theory to include dispersion interactions.[30] The experimentally determined apparent activation energy at 350 °C of 58 kJ/mol for H-ZSM-5 agrees with the theoretical value of 51 kJ/mol (at the ωB97X-D/6-31+g(d) level). Expressed in Gibbs free energies, the experimental apparent barrier coincides with the theoretically predicted 147 kJ/mol. The calculation was restricted to the concerted pathway, in view of the experimental kinetic measurements favoring the direct concerted mechanism.[21,22]

Although fairly good agreement with experimentally measured kinetics has been achieved in the study of Van der Mynsbrugge et al. in ref 29, the applied static approach, describing the transition state as a single structure corresponding to a first-order saddle point on the potential energy surface, considered only one methanol and one benzene molecule interacting at the active site. Notably, two significant aspects are not accounted for in this static approach: the thermal fluctuations of the flexible zeolite framework and the presence of additional solvent molecules inside the pores of the material. The importance of the framework flexibility has been duly recognized, but molecular dynamics simulations are required to quantify its effect on the kinetics of chemical reactions taking place in the voids of the nanoporous catalyst.[31−33] The assumption of a single methanol molecule per active site may hold under the conditions employed in experimental kinetic studies, which are typically performed at atmospheric pressure using dilute reagent streams at high feed rates to inhibit secondary reactions, and allows the kinetics of individual elementary steps to be investigated. However, in industrial MTO processes, more severe conditions are applied, and methanol conversion may occur at elevated pressures and temperatures,[34−36] with water often present in the methanol feed. Higher methanol partial pressures during the contacting step improve the overall efficiency of the process,[37,38] while adding process condensate or steam to the system allows increasing the selectivity toward lighter olefins.[3] In particular, tuning of the ethene to propene ratio by diluting the methanol feed with water has been investigated in several studies.[12,39−42]

The presence of additional methanol or water molecules can affect the overall catalytic performance of the zeolite material because these protic solvent molecules can interact through hydrogen bonding, both with each other and with the Brønsted acid sites of the catalyst.[43] In this paper, we employ a metadynamics simulation technique to account for these effects by sampling free energy surfaces in a multidimensional coordinate space spanned by several generalized collective variables to describe the complex reaction coordinate. Thus far, approaches involving ab initio molecular dynamics have hardly ever been applied in computational heterogeneous catalysis;[44−48] it is, however, particularly promising in view of the complexity of processes taking place inside the pores of a solid catalyst.

In the present study, the influence of the methanol loading on the mechanism of benzene methylation with methanol in H-ZSM-5 is investigated. First, the formation of protonated hydrogen-bonded methanol clusters at the active sites is discussed. Second, the reactivity of these methanol clusters toward benzene methylation is studied. In particular, the influence of the orientation of the methanol cluster with respect to the benzene molecule and the Brønsted acid site is assessed. Focusing on the extraction of forward free energy barriers and intrinsic rate coefficients for the methylation of benzene with methanol in H-ZSM-5, we aim to get more insight into the possible methylation mechanisms and to identify the factors determining the preferred mechanism and the activation free energy. The outcome of the metadynamics simulations is compared with previous results obtained using a static approach.[29] The molecular dynamics approach is shown to provide more detailed insights into the mechanism of benzene methylation, and allows exploring alternative pathways, which were previously overlooked in the simplified static model.

2. COMPUTATIONAL METHODS

First, equilibrium ab initio molecular dynamics (AIMD) simulations of the reactant state basin were carried out. Next, several metadynamics (MTD) simulations were performed, with different degrees of methanol loading, and different orientations of the attacking methanol. To rationalize on the effect of the zeolite catalyst, the reaction was also performed in pure methanol solvent. Although most attention is given to the direct mechanism for methylation, a comparison was also made with the stepwise mechanism. Finally, all here obtained data are compared with the results of static gas phase cluster calculations to assess the influence of confinement and framework flexibility.

2.1. Ab Initio Molecular Dynamics. To fully account for the flexibility of the zeolite host and the dynamics of the guest molecules, ab initio molecular dynamics (AIMD) simulations are performed by means of density functional theory (DFT) calculations in a fully periodic H-ZSM-5 catalyst model. H-ZSM-5 exhibits the MFI topology, characterized by perpendicularly oriented intersecting straight (5.3 × 5.6 Å) and zigzag channels (5.1 × 5.5 Å), made up of 10 rings and forming a three-dimensional medium-sized pore system.[49] To make the material active for catalysis, a substitutional defect is introduced by replacing one Si atom with an Al atom. The introduced negative charge is compensated by a proton, thereby creating bridging Si−OH−Al groups or so-called Brønsted acid sites.[1] The orthorhombic MFI unit cell, containing 96 T atoms, was taken from ref 49. The Al defect was placed on the T12 site,[49] creating a Brønsted acid site at the channel intersection, which offers maximal available space to the guest molecules. AIMD

dx.doi.org/10.1021/cs400706e | ACS Catal. 2013, 3, 2556−2567

simulations were performed with the CP2K simulation package[50] on the DFT level of theory and with Gaussian plane wave basis sets (GPW).[51,52] The revPBE functional was chosen for its improved catalytic energies compared with the commonly used PBE functional for solid-state calculations.[53] The DZVP-GTH basis set[54] was used, and Grimme D3 dispersion corrections[55] were added. The time step for integration of the equations of motion was set to 0.5 fs. The system was equilibrated for 5 ps, followed by a production run of 45 ps at 670 K and 1 bar in the NPT ensemble.

2.2. Metadynamics. Benzene methylation reactions (Scheme 1a) were investigated with the MTD approach at

Scheme 1. (a) General Reaction Scheme for Benzene Methylation with Methanol[a] and (b) Schematic Representation of the Transition State for the Concerted Mechanism and the First Step of the Stepwise Mechanism[b]

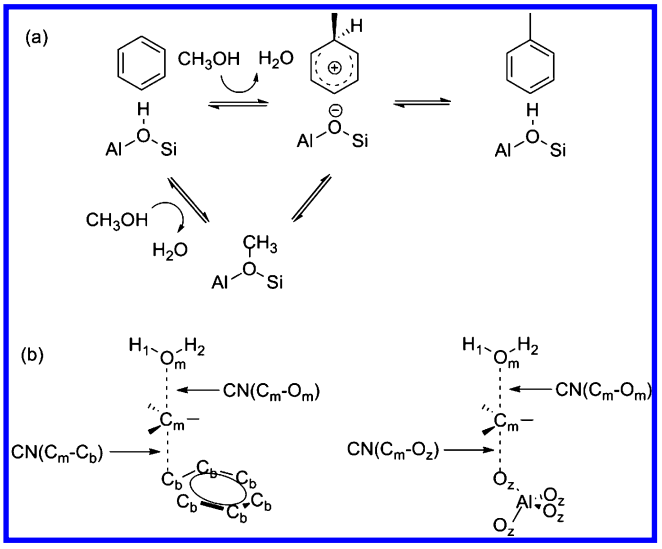

[a]The concerted mechanism involves electrophilic addition, followed by proton elimination. In the stepwise mechanism, the methyl group of methanol is transferred to the zeolite framework prior to the actual benzene methylation. [b]Atom labels and collective variables as referred in the text.

670 K, a temperature that matches industrial MTO setups, in the NVT ensemble. The MTD method was first introduced by Laio and co-workers and enables efficient computation of free energies of complex systems.[56] The method is especially suited to explore new reaction pathways by identifying a set of collective variables that allow sampling interesting regions of the potential energy surface.[57,58] For the simulation of chemical reactions, it is especially useful to use coordination numbers as collective variables.

The cell parameters, taken from the NPT simulation, are as follows: $a = 20.3528$ Å, $b = 20.2144$ Å, $c = 13.6141$ Å, and $\alpha = \beta = \gamma = 90°$. Gaussian hills are spawned along two collective variables (CV), defined by coordination numbers (CN):

$$\mathrm{CN} = \sum_{i,j} \frac{1 - (r_{ij}/r_0)^{nn}}{1 - (r_{ij}/r_0)^{nd}} \quad (1)$$

where the sum runs over two sets of atoms i and j and r_{ij} is the distance between atoms i and j.

r_0 is a reference distance, which depends on the bond type described by the CN. The parameters nn and nd are set to 6 and 12, respectively, ensuring a value of 0.5 for each CN term at the reference distance and a fast decaying value at larger distances. Quadratic walls were used to restrict the simulations to an area of interest on the free energy surface, as schematically depicted in Figure 1. A summary of the parameters identifying the CVs and the applied walls is given in Supporting Information Table S1.

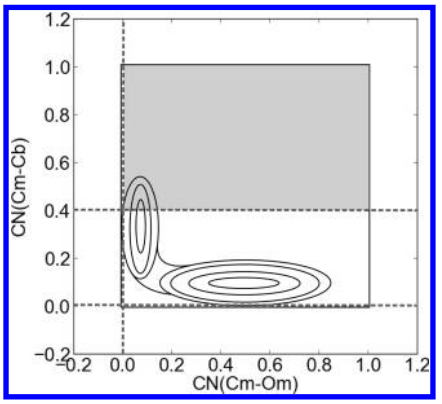

Figure 1. Schematic representation of the two-dimensional free energy profile of the benzene methylation reaction in H-ZSM-5, with indication of the position of the quadratic walls (dashed lines) to keep the simulation out of the gray shaded area.

The majority of the simulations performed in this paper use a set of collective variables that enable the simulation of the concerted methylation mechanism. However, some simulations were also performed on the stepwise mechanism, in which first a methoxy species is created (Scheme 1b). For both mechanisms, the first CV (CV1) is defined by the CN between the reacting methanol's carbon (C_m) and oxygen (O_m) atoms (see Scheme 1b). The equilibrium C_m-O_m bond length in protonated methanol amounts to ~1.5 Å, as determined by our static calculations, which justifies the choice of r_0 as 1.59 Å. As the C_m-O_m bond breaks in both mechanisms with the formation of water in the product state, a single-sided quadratic potential energy wall was placed at position CN1 = 0.01 (Figure 1), which corresponds to a bond length of 3.42 Å. This barrier prevents water escape and enhances the probability of a transition state recrossing. The latter is important to produce a statistically relevant sampling of the transition state region.

The second CV (CV2) depends on the reaction mechanism under study. In the direct, concerted mechanism, CV2 is defined by the CN between C_m and the six benzene carbon atoms (C_b) (Scheme 1b). In protonated toluene, the C−C bond length is 1.57 Å, justifying the use of $r_0 = 1.59$ Å as reference distance for this CN. Similar to CN1, a single-sided quadratic wall is placed at CN2 = 0.008 (Figure 1) to keep the distance between the methyl carbon and the benzene molecule under control. In addition, a repulsive quadratic wall is introduced at CN2 = 0.4 (C_m-C_b bond distance ~1.7 Å; Figure 1), promoting in this way a TS recrossing, since in the TS-to-toluene, the forming C_m-C_b bond length amounts to ~2.1 Å. Moreover, without this additional wall, low-activated proton hopping to one of the neighboring C_b atoms and deprotonation of the toluenium ion (second step in Scheme 1a) occurs readily, making a recrossing of the TS for the methylation more problematic.

The shapes of the applied walls are illustrated in Figure S1. In the stepwise mechanism, the CN between C_m and the four zeolite oxygen atoms (O_z) bonded to the Al atom is considered as the CV2 (Scheme 1b). Here, the quadratic walls and r_0 are

dx.doi.org/10.1021/cs400706e | ACS Catal. 2013, 3, 2556−2567

placed at positions identical to those in the concerted mechanism. To ensure that the reacting methanol is always in its reactive (protonated) state, two additional walls were placed on the CN between O_m and the two H atoms bonded to it (H_1, H_2) at 0.03 with r_0 = 1.0 Å, which corresponds to a Om−H distance of 1.8 Å. The width of the Gaussian hills was set to 0.02. The height of the hills was initially 0.05 eV (4.8 kJ mol^{-1}). After the first and second recrossing of the transition state, the hill height was reduced to 0.025 and 0.0125 eV, respectively. A new hill was spawned every 50 time steps. The MD time step was again set to 0.5 fs for all MTD simulations. The MTD simulations were continued until a statistical error of <5 kJ/mol on the barrier height and varied between 42 and 80 ps.

After a MTD simulation, the free energy profile of the reaction can be reconstructed on the basis of the sum of the spawned Gaussian hills. The free energies were calculated as the mean free energy over the part of the simulation where the barrier height starts to fluctuate and the dynamics along the reaction coordinate become diffusive (Supporting Information Figure S2). The statistical errors were computed as the standard deviation of the mean after removal of correlated data values.[57] Free energy barriers ($\Delta G^{\ddagger}$) were computed after projecting the 2D free energy surface onto a 1D surface, taking the difference (CV2 − CV1) as the reaction coordinate:

$$G(\mathrm{CV2}-\mathrm{CV1}) = -\frac{1}{\beta} \ln\{\int_{-\infty}^{\infty} \mathrm{d}_{\mathrm{CV1}} \exp[-\beta G(\mathrm{CV2}-\mathrm{CV1}, \mathrm{CV1})]\} \quad (2)$$

The $\Delta G^{\ddagger}$ values were calculated as the difference between the free energy of the transition state ensemble and the free energy of the reactant region on the 1D free energy surface:

$$\Delta G^{\ddagger} = -\frac{1}{\beta} \ln \frac{\exp[-\beta G(TS)]}{\int_{-\infty}^{TS} \exp[-\beta G(s)]\, \mathrm{d}s} \quad (3)$$

where $\beta = 1/k_B T$, and TS is the position at the top of the barrier along the reaction coordinate (s). On the basis of the obtained free energy barriers for the reaction, intrinsic, unimolecular rate coefficients (k) were calculated using standard transition state theory:

$$k = \frac{1}{\beta h} \exp(-\beta \Delta G^{\ddagger}) \quad (4)$$

2.3. Static Calculations. To compare the results from the molecular dynamics simulations with static approaches, a series of extended cluster DFT calculations were also performed with the Gaussian 09 software package[59] (Supporting Information). Thereby, the H-ZSM-5 catalyst is represented by an extended 46T cluster containing one acid site (see ref 29 for details). ONIOM(PBE/6-31+g(d):PM3) geometries are combined with PBE/6-311+g(d)-D energies, which is an approach similar to those applied in our earlier papers.[27,29] The PBE functional is used to allow comparison with the periodic molecular dynamics calculations. Dispersion is accounted for by means of D3 corrections as proposed by Grimme and co-workers.[55] Free energies and entropies were obtained with our open source software package, Tamkin.[60,61] We also report coordination solvation-free energies and enthalpies, which were calculated at the PBE/6-311+g(d,p) level of theory. The coordination solvation free energy[62] was calculated as CSG = G[$(MeOH)_nH^+$] − nG[MeOH], with n the number of methanol molecules in the protonated methanol cluster. For the calculation of the coordination solvation free energies, we included polarization functions for hydrogen because this resulted in a better convergence for the gas phase calculations of charged compounds.

3. RESULTS AND DISCUSSION

3.1. Methanol Clustering. Previous computational studies on the methylation reaction[26−29] took into account the presence of only one methanol molecule. However, higher loading of methanol makes a significant difference in the chemical system under study, as shown by ^{1}H MAS NMR experiments on deuterated methanol in H-ZSM-5.[63] Hunger et al. performed multinuclear solid-state NMR spectroscopy and temperature-programmed desorption experiments on methanol in H-ZSM-5 and observed the formation of protonated methanol clusters at high methanol loadings.[64,65] Notably, at higher loadings, the acid proton of the zeolite may be transferred to methanol, whereas at low methanol loadings, only physisorbed methanol is present. This is attributed to the higher proton affinity of large methanol clusters in comparison with smaller adsorbate complexes. A similar study was performed to assess the tendency of water to form clusters in H-ZSM-5.[66] In an earlier computational study, Termath et al.[67] concluded that deprotonation of H-SAPO-34, a silicoaluminophosphate zeotype catalyst with CHA topology, is enhanced by the formation of water clusters as the proton affinity increases with cluster size. Hybrid MP2:DFT calculations have shown that proton transfer occurs from a protonated zeolite to a molecule or a cluster of molecules with a proton affinity comparable to or larger than that of ammonia.[68] Because of this cluster formation, typical for protic solvents, the mobility of the catalyst's acidic proton is greatly enhanced. For example, neutron Rietveld experiments recently revealed high acidic proton mobility in low-silica ferrierite, which could be explained by a proton transfer mechanism in which water molecules or clusters act as proton carriers.[69] This behavior is expected to have a major influence on zeolite-catalyzed reactions.

To investigate the location of the acidic proton and the degree of methanol clustering, a high temperature (670 K) 45 ps MD production run was performed on the H-ZSM-5 catalyst, loaded with 5 methanol molecules and 1 benzene molecule. To perform a statistical analysis of specific geometrical features, snapshots were taken every 1 fs, yielding an ensemble of 45 000 conformations of molecules residing in the voids and channels of the catalyst. This analysis reveals that the acidic proton, initially located on one of the four zeolite oxygen atoms surrounding the Al substitution, quickly migrates to a cluster of H-bonded methanol molecules residing close to the acid site. Proton transfer from the cluster back to the zeolite occurs rarely (∼0.3%), meaning that the methanol cluster stays essentially protonated throughout the entire simulation. Thus, the acidic proton effectively becomes mobile at higher methanol loadings. In the relatively short (45 ps) simulation, the protonated cluster remains in the vicinity of the Al site, often hydrogen-bonded with one of the deprotonated framework oxygen atoms (∼33% probability).

Using a summed (donor-H + H-acceptor) distance less or equal to 3.5 Å as a criterion for H-bonding, the probabilities of occurrence of various methanol clusters are shown in Figure 2. A high degree of methanol clustering is observed, a protonated methanol trimer having the highest probability of occurrence. This trimer is found in the channel intersection, with the individual monomers pointing toward the straight and zigzag

dx.doi.org/10.1021/cs400706e | ACS Catal. 2013, 3, 2556−2567

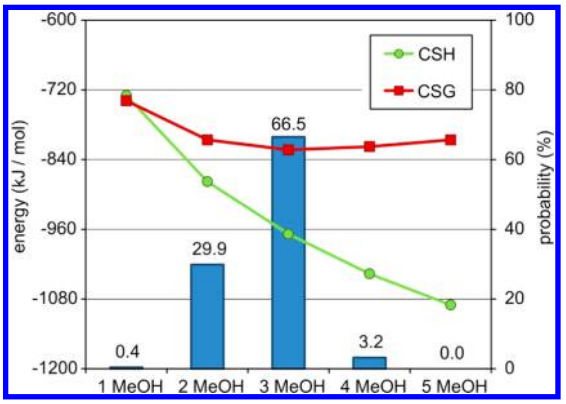

Figure 2. Probabilities of protonated methanol cluster sizes encountered in the MD simulation (bar chart), coordination solvation free energy (CSG), and enthalpy (CSH) in kJ/mol.

channels (Figure 3). Proton mobility did not occur in a 45 ps MD simulation loaded with only one methanol in the unit cell. In this

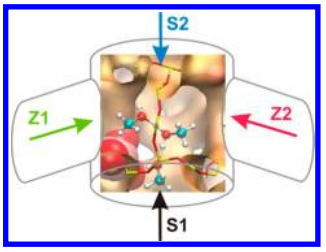

Figure 3. Protonated methanol trimer inside the channel intersection. Each of the three methyl groups points toward one of the four channel entrances, indicated by the straight channel vectors S1 and S2, and zigzag channel vectors Z1 and Z2. The AlO_4 site is represented as van der Waals spheres, with the central Al atom colored pink.

case, methanol remains physisorbed to the zeolite framework. To obtain more insight into the driving force for the preferential methanol trimer formation, it is interesting to calculate the gas phase coordination solvation free energy of an excess proton in methanol, that is, the free energy of interaction of a proton with a given number of methanol molecules in the protonated methanol cluster (see Supporting Information Figure S3 for the optimized clusters).

Figure 2 depicts the coordination solvation free energy (CSG) and its enthalpic contribution (CSH). It can be concluded that the primary solvation shell of the proton is formed by three methanol molecules as the CSG value is minimal for trimeric protonated methanol clusters. However, the CSH values further decrease with the formation of larger clusters, indicating that the entropic penalty largely prevents the formation of clusters with more than three methanol molecules.

Our current findings are in line with previously reported results. Grimsrud et al. investigated the proton solvation energies with various solvents in gas phase ion equilibria studies. They observed a significant decline of the stabilization per methanol molecule beyond trimeric clusters.[70] Chang et al. used the B3LYP functional in their ab initio study of proton migration in cyclic and linear protonated methanol clusters.[71] More recently, Fifen et al. performed static calculations on neutral and protonated methanol clusters using both the B3LYP and M06-2X functionals combined with an implicit solvent model to determine the solvation free energy of the proton in methanol.[72] Both of these theoretical studies confirmed the experimental findings on the importance of protonated methanol trimers.

Similarly, proton solvation by water shows a preference for tetrameric clusters.[70] This cluster formation in water was shown to lie at the basis of the solvation and transport of an excess proton in bulk water. The most favorable solvation structure for a hydrated proton was shown to be a distorted Eigen-type complex ($H_9O_4^+$) in which the excess proton is dynamically delocalized among three water molecules around a central hydronium ion (H_3O^+). At any given instant, one of the H-bonds between H_3O^+ and the three water partners is considerably shorter than the two others. The exceptionally high diffusion of protons originates from a combination of proton hopping or shuttling between molecules and the translational diffusion of the solvation complex.[73] Analogous to the protonated water clusters, in our simulation, trimeric methanol clusters most frequently adopt a distorted Eigen complex, one of the H-bonds between the central methoxonium and the two methanol partners being considerably closer than the other (Supporting Information Figure S4).

3.2. Benzene Orientation. Alongside the behavior of the methanol molecules inside the H-ZSM-5 catalyst, the position and orientation of the adsorbed benzene molecule is assessed on the basis of the high-temperature MD simulation. The benzene molecule is located in a channel intersection, distant from the Al defect. Herein, the orientation of the aromatic ring is not randomly distributed. Figure 4 displays the probability

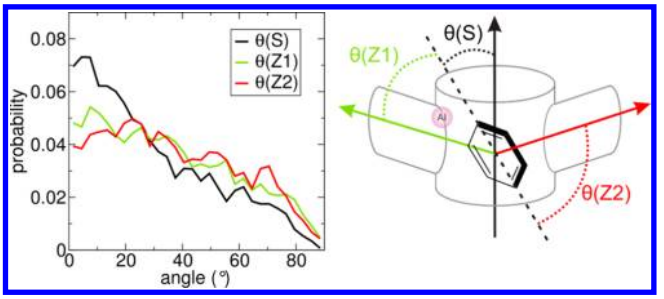

Figure 4. Probability distribution of the angle θ between the plane of the aromatic ring and three channel vectors.

distribution of the angle θ between the plane of the benzene molecule and the channel vectors. There is a clear preference for small angles, meaning that the benzene ring is mostly oriented along the axis of one of the channels connected with the channel intersection. The strongest preference for small angles is observed for the straight channel, which is due to the 105° angle between the zigzag channels Z1 and Z2. The benzene ring can at any given time be aligned with the straight channel and either Z1 or Z2, but not with both Z1 and Z2. Although there is a preference for orientations with small θ(S) angles from the 2D correlation histograms, it is clear that all possible combinations of two angles are accessible because the benzene molecule has enough room to rotate freely inside the channel intersection (Figure S5).

The preference of the benzene ring for an orientation parallel to the three channel vectors represents an additional barrier that has to be overcome in the methylation reaction, which requires a larger angle between the benzene ring and the channel vectors (Figure 7c). During MTO conversion, the aromatic substrates for methylation in H-ZSM-5 are xylenes and tri- and tetramethylbenzenes.[74] These bulkier aromatics are expected to adopt even more selective orientations, which may strongly affect the methylation rates of these substrates. However, a study

dx.doi.org/10.1021/cs400706e | ACS Catal. 2013, 3, 2556−2567

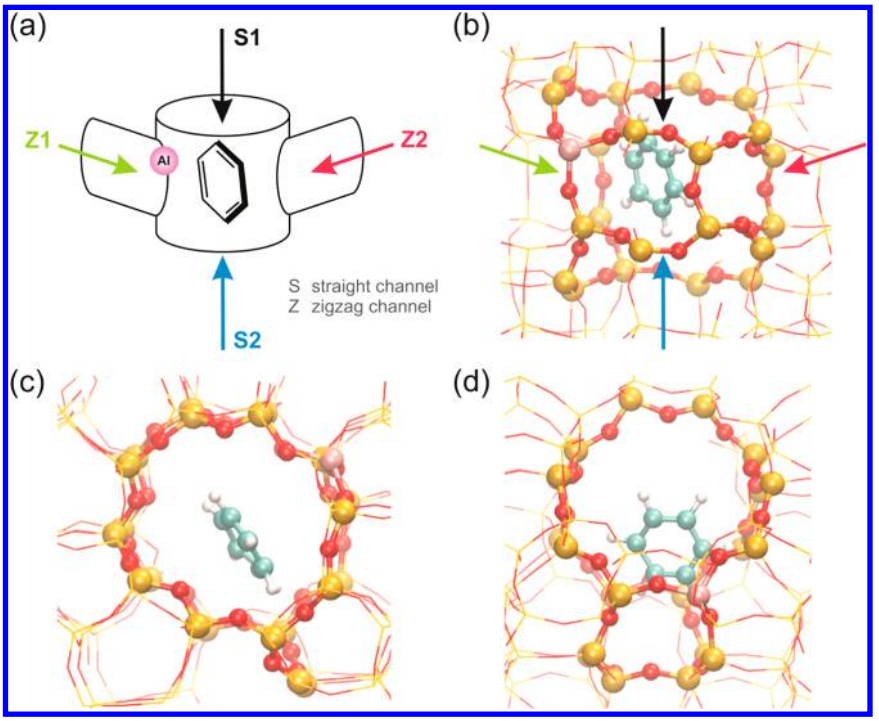

Figure 5. H-ZSM-5 channel intersection containing a benzene molecule. (a) Schematic representation of the channel intersection. The arrows indicate the channel vectors of the straight channel (black and blue arrows) and the two connecting zigzag channels (red and green). (b) Same orientation as in panel a. (c) Seen along channel S1. (d) Seen along channel Z1. The five methanol molecules are omitted from the figure for clarity.

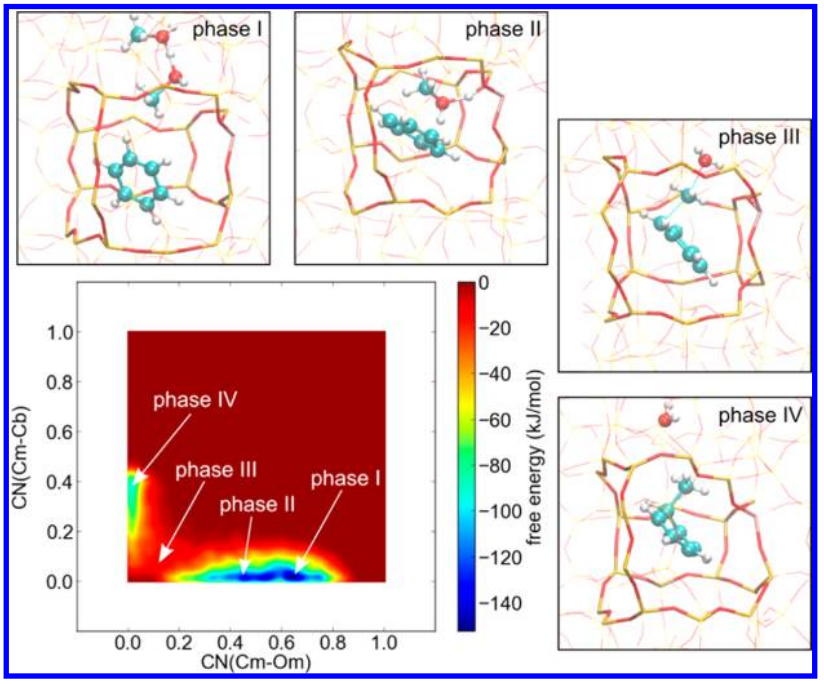

Figure 6. Two-dimensional free energy surface from MTD, with selected conformations representing the four phases along the reaction pathway. Methanol molecules that do not participate in the reaction are not shown.

of the methylation of methylated benzene compounds is beyond the scope of this work.

3.3. Benzene Methylation at High Methanol Loadings.

As mentioned above, at industrially relevant conditions, methanol molecules are likely to form protonated and H-bonded clusters inside the H-ZSM-5 catalyst. This cluster formation is expected to have an influence on the reactivity of methanol. Therefore, the methylation of benzene in H-ZSM-5 is studied with five methanol molecules present in and around the channel intersection where the reaction will take place. A MTD simulation was performed on the concerted mechanism with two collective variables (CV), defined by coordination numbers corresponding to breaking of the C_m-O_m bond (CV1) and the formation of a C_m-C_b bond (CV2). During the MTD simulation, the benzene molecule is located in the channel intersection close to the Al defect, and the reacting methanol is

dx.doi.org/10.1021/cs400706e | ACS Catal. 2013, 3, 2556−2567

located in the straight channel (S1 in Figure 5), adjacent to the channel intersection. Initially, the remaining four methanol molecules were placed randomly inside the zeolite pores. No restrictions were imposed on the methanol cluster size, allowing H-bonds between methanol molecules to be formed and broken. The resulting two-dimensional free energy surface shows two separate low-energy regions, corresponding to the reactant and product states (Figure 6).

We modeled the methylation reaction according to the concerted reaction mechanism. From the 2D free energy surface (Figure 6), we can conclude that the reaction has an asynchronous character because the methanol carbon−oxygen bond is largely broken when the new carbon−carbon bond is being formed. As a result of the clear separation of the reaction pathway into two distinct parts, an approximate one-dimensional profile can be constructed by taking the difference of the two CVs, which projects the 2D surface onto the diagonal CV2−CV1, running from the bottom-left to the top-right (Figure 7a).

Along the reaction pathway, four phases can be distinguished (Figure 6): (I) Initially, the reacting, that is, protonated, methanol is located in the straight channel. Steric restrictions imposed by the confinement of the channel disfavor the formation of trimeric clusters. Thus, an H-bonded dimer is formed with a nearby methanol molecule. (II) As the C_m−O_m bond is weakened by the Gaussian hills and the reacting methanol approaches benzene in the channel intersection, H-bonding with the neighboring methanol diminishes to about 20% probability and is replaced by an H-bond with the nearby acid site (Figure 7b). Benzene adopts a configuration appropriate for reaction. (III) At the transition state region, further weakening of the C_m−O_m bond and breaking of all H-bonds to ∼10% probability (Figure 7b) allows dissociation of the methyl cation from the reactive protonated methanol toward one of the benzene C_b atoms. (IV) Finally, formation of the C_m−C_b bond yields the toluenium and neutral water reaction products.

The forward reaction with five methanol molecules and reaction from the S1 channel exhibits a free energy barrier of 137 ± 3 kJ/mol and an intrinsic rate coefficient between 1.7×10^2 and 5.0×10^2 s^{-1} (Table 1). These values are in close agreement with the intrinsic free energy barrier (142 kJ/mol) and corresponding *k*-value at 673 K (1.2×10^2 s^{-1}) that have recently been predicted in the extended-cluster calculation of Van der Mynsbrugge et al.[29]

As indicated in the previous section, the orientation of the benzene molecule with respect to the straight and zigzag channels is an important aspect. In Figure 7c, the mean angle θ between the plane of the benzene ring and the channel vectors is plotted along the reaction coordinate. Before the transition state region, θ is preferentially below 45°. However, when approaching the transition state of the methylation reaction, the orientation of the benzene ring has to increase to 56° at the transition state region. A comparable angle of 54° is found in our static 46T cluster transition state calculation.

3.4. Methanol Attack from the Four Different Channels. With the benzene molecule placed inside the channel intersection wherein the Al defect is present, the reacting methanol may attack from the 4 channels (S1, S2, Z1, and Z2 in Figure 5) connected to this channel intersection. To investigate the effect of the origin of attack, the MTD simulation was repeated with the protonated methanol initially located in one of the four channels, using the same MTD parameters. As shown in Figure 8, the origin of attack strongly influences the free energy profile. The differences in the reaction barriers can be easily

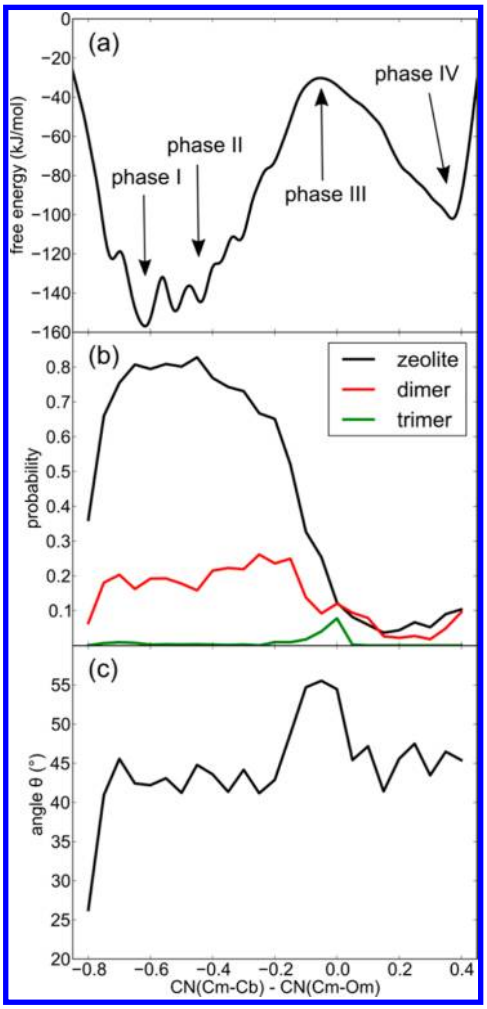

Figure 7. (a) One-dimensional free energy profile, derived from the 2D surface (Figure 6) as the difference between the two CVs. The second minimum at around 0.4 is an artifact of the wall at CN2 = 0.4. (b) Degree of H-bonding of the reacting methanol with the zeolite acid site (black) or with one (red) or two (green) methanol molecules, and (c) angle θ between the benzene ring plane and the straight channel vector (see Figure 4), plotted along the 1D MTD reaction coordinate, with methanol attacking from the S1 channel. Values were taken as the mean over the last part of the MTD trajectory starting at the first TS recrossing.

Table 1. Free Energy Barriers (kJ/mol) and Intrinsic Rate Coefficients (s^{-1}) at 670 K for MTD Simulations of the Methylation of Benzene with a Varying Number of Methanol Molecules Per Unit cell

	$\Delta G^{\ddagger}$ (kJ/mol)	k (s^{-1})
1 MeOH	118 ± 5	(3.6×10^3)−(2.2×10^4)
2 MeOH	122 ± 1	(3.6×10^3)−(5.1×10^3)
3 MeOH	154 ± 4	(6.7×10^0)−(2.8×10^1)
5 MeOH−S1	137 ± 3	(1.7×10^2)−(5.0×10^2)
5 MeOH−S2	103 ± 4	(6.4×10^4)−(2.7×10^5)
5 MeOH−Z1	148 ± 2	(2.8×10^1)−(5.8×10^1)
5 MeOH−Z2	122 ± 2	(3.1×10^3)−(6.2×10^3)
5 MeOH−NB	146 ± 2	(4.0×10^1)−(8.3×10^1)
MeOH solvent	147 ± 3	(2.8×10^1)−(8.3×10^1)
5 MeOH, stepwise[a]	152 ± 3	(1.2×10^1)−(3.4×10^1)

[a]Framework methoxide formation.

dx.doi.org/10.1021/cs400706e | ACS Catal. 2013, 3, 2556−2567

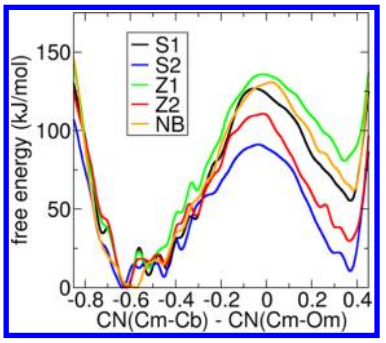

Figure 8. 1D free energy profiles for benzene methylation with a loading of five methanol molecules per unit cell and methanol attacking from channels S1, S2, Z1, Z2 or a neighboring channel intersection without Al substitution (NB).

explained by the stability of the reactants. When the reacting methanol approaches the benzene ring from the opposite side of the Al defect (S2 or Z2), a destabilizing charge separation is present in the reactant state between the negatively charged Al site and the protonated methanol. The lowest free energy barrier, 103 kJ/mol (Table 1), is observed for the case in which methanol attacks from channel S2 (see the blue arrow in Figure 5), followed by 122 kJ/mol from channel Z2 (red arrow), which is in line with a larger distance between the charged groups in the case of the S2 attack. The enhanced stabilization of the transition state and product state regions relative to the reactant state region after methanol attack from channels S2 or Z2 is clearly visible in the red and blue free energy profiles in Figure 8.

3.5. Methylation of Benzene in a Neighboring Channel Intersection. The orange free-energy profile in Figure 8 corresponds to the reaction with benzene located in a neighboring channel intersection without Al substitution at a distance of about 10 Å from the channel intersection in which the aluminum defect is present. Here, the reacting (protonated) methanol has to diffuse from the acid site where it got protonated, through the straight channel (S1), to the benzene molecule. In this case, again, a good electrostatic interaction between the negatively and positively charged centers in the transition state and product state is prevented, leading to higher values of the activation free energy. This simulation clearly demonstrates that methanol clusters are relatively mobile in H-ZSM-5, which suggests that the exact locations of the Al sites and, hence, the Brønsted acid protons, are not crucial for the methylation reaction, as long as the acidic proton is accessible to the methanol molecules.

3.6. Effect of Protonated Methanol Clusters on the Methylation of Benzene. To investigate the effect of methanol clustering on the free energy barrier of the benzene methylation reaction, metadynamics simulations were performed with one, two, and three methanol molecules, respectively, inside the nanopores of the catalyst. To simulate the effect of explicit methanol clustering throughout the simulation, the methanol molecules were held together as a single cluster throughout the simulation. To this end, single-sided quadratic walls were placed on all O−H bonds in the cluster, keeping the reacting (terminal) methanol oxygen bonded to two H atoms (CN = 0.03, r_0 = 1.0 Å). The resulting one-dimensional free energy profiles are shown in Figure 9. Methylation with the monomer is most favorable, the free energy barrier for methylation being about 4 and 36 kJ/mol lower than the dimer and the trimer, respectively (Table 1). With a higher methanol loading, the zeolite's acidic proton is

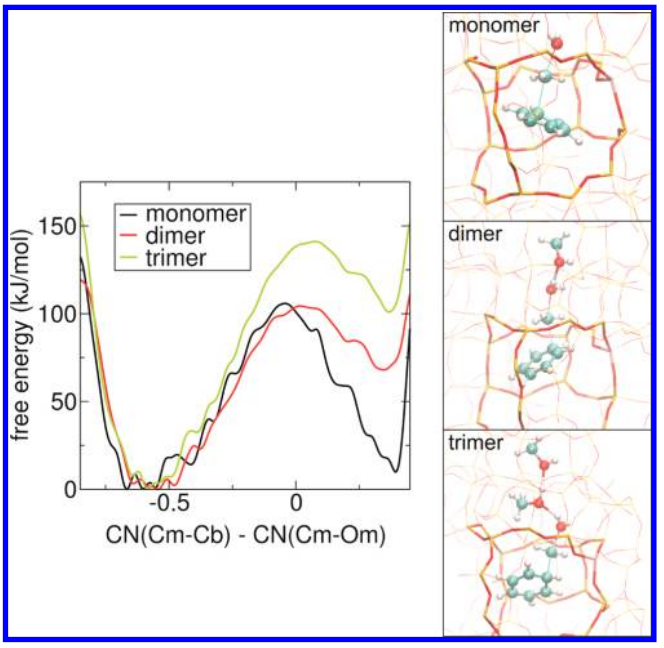

Figure 9. Free energy profiles of the methylation of benzene with protonated methanol restrained to a monomer, dimer, and trimer cluster, with snapshots illustrating the respective transition states.

transferred to the H-bonded methanol cluster, hence, inducing a delocalization of the positive charge. This results in an enhanced stabilization of the methanol cluster, and as such, its reactivity is also decreased. Thus, methanol clustering negatively affects the reactivity of methanol toward benzene methylation. Note that the free energy barrier for the methanol trimer is similar to that of the simulation with five methanol molecules, on which no clustering restraints were imposed. The fact that methanol trimers exhibit the highest probability to be formed (see Figure 2) explains this observation. From Figure 9, it can also be concluded that with an increasing methanol cluster size, the position of the transition state shifts toward the product state. This can be understood by the formation of a neutral water−methanol cluster as a result of the imposed clustering restraint. As shown in Figure 7b, the reacting methanol molecule prefers to be free from H-bonding with methanol around the transition state. Thus, the clustering restraint induces a destabilization of the transition state region.

Previous modeling works, based on static approaches, usually assumed a single methanol molecule H-bonded to the acidic zeolite proton to be the reactive species.[26−29] Although the activation energy is, indeed, lowest for a single methanol molecule, the tendency to form a protonated methanol cluster will also affect the overall reactivity and should be included in the simulations to obtain more realistic reaction paths. Using static approaches, inclusion of extra methanol molecules becomes cumbersome because the position of these species is not straightforward and can no longer be represented by considering one point on the potential energy surface (see section 3.7).

3.7. Influence of Molecular Environment and Molecular Dynamics on Calculated Reaction Kinetics. At this stage, it is interesting to obtain insight into the several factors controlling the overall reaction barriers and kinetics of the reactions under study. We distinguish several important effects: the number of methanol molecules in the reactant phase, the presence of the zeolite framework, and the zeolite's framework flexibility. The importance of each of these effects can be

dx.doi.org/10.1021/cs400706e | ACS Catal. 2013, 3, 2556−2567

assessed, and therefore, the same set of reactions as discussed in the previous section (i.e., the methylation of benzene with a single methanol molecule, methanol dimer or trimer) will be investigated. For this assessment, we also performed static calculations, the results of which will be compared with the metadynamics simulations of the same reactions. First of all, the reactions were modeled with a static approach in the gas phase using a protonated methanol molecule, dimer, or trimer as methylating agent without accounting for the zeolite surroundings. Second, static calculations are performed on a large finite 46T cluster, which is a methodology that was earlier applied in references 27 and 29. In addition, we also performed a MTD simulation of the methylation of benzene in an explicit methanol solvent model to assess the impact of the confined zeolite environment on the reaction barrier. The resulting free energy barriers with the various simulation techniques are schematically represented in Figure 10.

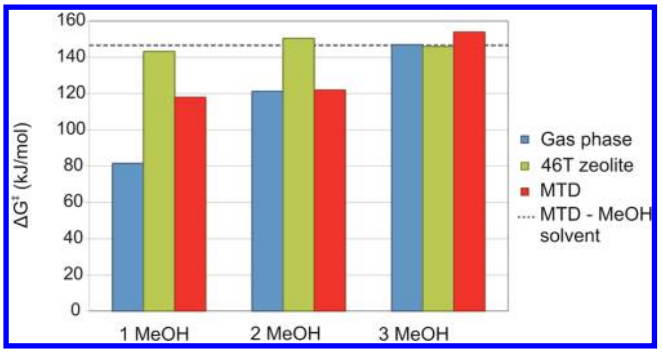

Figure 10. Free energy barriers (kJ/mol) at 670 K for the methylation of benzene with one, two, or three methanol molecules modeled in gas phase, a 46T cluster representing H-ZSM-5, and with metadynamics, including the periodic framework or in methanol solvent.

In the gas phase calculations, the free energy barriers for the benzene methylation (blue bars in Figure 10) increase with an increasing number of methanol molecules (82, 121, and 147 kJ/mol for one, two, and three MeOHs, respectively). Calculation of the coordination solvation free energy of an excess proton in methanol (Figure 2) showed that every additional methanol molecule induces an extra stabilization of the proton until three methanol molecules surround the proton. This increased stability of the protonated methanol clusters, as compared with a protonated methanol molecule, is reflected in significantly lower reactivity and higher free energy barriers for methylation at 670 K (Figure 10). The protonated methanol molecule is very reactive, leading to a very low free energy barrier. The higher free energy barriers for methylation from a methanol dimer and trimer are due to higher enthalpic contributions, not due to entropic effects to the reaction (Supporting Information Table S2). However, a significant entropic penalty is observed for the formation of the protonated methanol dimers or trimers starting from a methoxonium ion and neutral methanol molecules, as the methanol molecules get more organized by hydrogen bonding (Supporting Information Table S3). These free energies corresponding to the formation of these protonated methanol clusters are not included in the free energies reported in Figure 10, as only intrinsic data are reported. The performed gas phase calculations start from a very reactive methoxonium ion or protonated methanol cluster, which is not a representative model for realistic reaction conditions.

In a subsequent series of simulations, the zeolite environment is accounted for by means of large 46T clusters (Supporting Information Figure S6; green bars in Figure 10). Some of the present authors applied this methodology to obtain kinetic data with near chemical accuracy for the methylation of alkenes[27] and of benzene[29] with methanol in H-ZSM-5. When a single methanol molecule acts as the methylating agent, the surrounding zeolite stabilizes the reactant such that the free energy barrier is 62 kJ/mol higher for the 46T cluster simulation compared with the gas phase result.

The methylation with a methanol dimer and trimer exhibit only slightly higher energy barriers compared with a methylation with a single methanol molecule (143, 151, and 146 kJ/mol for one, two, and three MeOHs, respectively), indicating that the stabilization of the surrounding 46T cluster is stronger than the additional stabilization due to the delocalization of the positive charge over several methanol molecules as a result of cluster formation. The free energy barrier of the 46T cluster calculation for the methylation with one methanol molecule agrees well with the earlier reported 142 kJ/mol in reference 29. It can be observed that the entropic contributions to the free energy barriers for the methylation reactions are larger compared with the gas phase results (Supporting Information Tables S2 and S4); however, it is expected that the major entropic effect will be found for the formation of the protonated methanol clusters. In the prereactive complexes in the 46T zeolite cluster, we observed a neutral methanol molecule or a neutral methanol dimer hydrogen-bonded to the acid site, or a protonated methanol trimer for the reaction with one, two, or three methanol molecules, respectively. As expected, the entropic penalty for the formation of a methanol dimer or trimer, starting from one single methanol molecule adsorbed in the 46T zeolite cluster and gas phase methanol molecules, is significantly higher than for the formation of protonated methanol clusters in the gas phase (Supporting Information Tables S3 and S5). Again, this effect is not included in the intrinsic free energy barriers reported in Figure 10.

Interestingly, the free energy barriers obtained with the metadynamics simulations (red bars in Figure 10) are considerably lower than those obtained with the static 46T cluster approach. However, the trend of increasing free energy barriers with an increasing number of methanol molecules can be found here, as well. Both the inclusion of the surrounding framework by means of a periodic model and the use of a dynamical method during the MTD simulations have a clear impact on the calculated free energy barriers. Not only does the metadynamics approach allow accounting for the framework flexibility of the zeolite, it also takes into account anharmonic effects[44] that are typically not included in the static calculations.

Caution is needed when interpreting these 46T cluster results. In these simulations, protonated methanol clusters have the tendency to align their oxygen backbone along one of the zigzag channels (Supporting Information Figure S7). Although 46T cluster simulations are valuable, the size of this cluster is not sufficient to give a good description of a methanol trimer as methylating agent for benzene in a channel intersection of H-ZSM-5. Moreover, static cluster calculations do not provide detailed insight into the mechanism of the methylation from these protonated methanol clusters. As discussed earlier in this paper, protonated methanol clusters have a highly dynamical character—that is, the acid proton is shuttled throughout the different methanol molecules, and the clusters can attack the benzene molecule from different channels—which cannot be

dx.doi.org/10.1021/cs400706e | ACS Catal. 2013, 3, 2556−2567

described within a static approach. These results highlight some shortcomings of static calculations for the study of the reactivity of protonated methanol clusters inside a nanoporous host material. However, the static approach with extended zeolite clusters remains a valuable tool to study reaction kinetics in less complex molecular environments.

In addition, the methylation of benzene was simulated inside a pure methanol solvent box to assess the influence of the confinement imposed by the zeolite on the reaction. The applied model consists of one protonated methanol molecule and a benzene molecule in a periodic methanol solvent box with the same dimensions as the H-ZSM-5 unit cell (see the Computational Methods section). The free energy barrier obtained from the methanol solvent MTD simulation (dashed line in Figure 10), 147 ± 3 kJ/mol, is higher than for the MTD simulations with one and two methanol molecules in H-ZSM-5, but is only slightly higher than the free energy barrier for the zeolite-catalyzed reaction with five methanol molecules (137 ± 3 kJ/mol). This can be understood when visualizing the degree of methanol cluster formation in the reactant phase for these two reactions (Supporting Information Figure S8). In the methanol solvent, the methylation reaction is performed mainly by protonated methanol dimers and trimers, whereas for the case with five methanol molecules per acid site in H-ZSM-5, mainly protonated methanol molecules that interact with the zeolite's acid site perform the reaction. The latter are more reactive and give rise to lower free energy barriers for methylation of benzene. These findings also indicate that for the methylation of benzene, the main functions of the zeolite are to provide the Brønsted acidic proton for the acid catalysis and the electrostatic surroundings. For this reaction, apparently, the effect of the confined space imposed by the zeolite is not crucial. However, for the bulkier methylbenzenes, this effect is known to play a more prominent role because it leads to transition state shape selectivity.[16] Note that the main purpose of the pure solvent simulation is to study the effect of the polar environment in the absence of confinement effects. It is not intended to propose a realistic model for a methylation experiment in methanol solvent because the metadynamics methodology used here does not account for all possible side reactions that may occur in the solvent.

3.8. Stepwise Mechanism. For zeolite-catalyzed arene methylations, two distinct reaction pathways have been identified: the stepwise and concerted mechanisms.[23] In the stepwise mechanism, methanol is dissociated and forms a surface-bound methoxy group and a water molecule (bottom of Scheme 1a, top row of Supporting Information Scheme S1).[23] This framework methoxide methylates an aromatic molecule (bottom of Scheme 1a, middle row of Supporting Information Scheme S1) adsorbed in the zeolite pore in a second step. In situ spectroscopic methods are valuable tools for the identification of reaction intermediates being formed inside the working catalyst under real-world reaction conditions.[75−77] In this manner, surface methoxy groups have been detected by in situ MAS NMR−UV/vis spectroscopy during the methanol conversion to olefins at high temperature range ($T \geq 523$ K), and were found to participate in the formation of hydrocarbon-pool species, mainly during the induction period of the MTO process.[78−80] These spectroscopic studies give evidence that methylation reactions may occur through the stepwise mechanism. One of the most recent spectroscopic studies on the stepwise and concerted methylation mechanisms has been performed by Svelle and coworkers.[81] Although FT-IR spectroscopy did not detect methoxy groups on Brønsted sites, the stepwise route could not be ruled out, because the concentration of the reactive framework methoxide is expected to be low under optimal reaction conditions. On the other hand, several experimental kinetic studies support a direct reaction mechanism not involving a methoxy intermediate.[21,22,82]

During the MTD simulations of the concerted mechanism, we observed that the methanol carbon (C_m) sporadically migrates to one of the zeolite oxygen atoms (O_z) coordinated with the Al atom, forming a framework methoxide. To avoid interference of this reaction in the analysis of the concerted mechanism, in these cases, the simulation was restarted at an earlier time step.

However, the observation that the framework methoxide can be formed without bias potential acting on the C_m−O_z bond suggests that the stepwise mechanism may be a plausible alternative route to the methylated benzene product, as well. Theoretical studies have shown that the methoxide formation step is the rate-determining step in the stepwise mechanism.[25,83] Therefore, we performed a separate MTD simulation to assess the feasibility of the methoxide formation, again with five methanol molecules and one benzene molecule present in the H-ZSM-5 unit cell. The resulting free energy barrier, 152 ± 3 kJ/mol (Table 1), is somewhat higher than most of the barriers obtained in the concerted pathway, in line with previous studies.[23] Given that methanol adsorbs much more strongly than benzene at acid sites, this result suggests that the stepwise mechanism may still compete with the concerted mechanism, especially at low benzene concentrations.

Recently, Svelle et al. proposed a third reaction mechanism for the methylation of highly substituted methylbenzenes. It differs from the direct and stepwise mechanisms in that the aromatic molecule resides in a protonated form as reaction intermediate, which is found stable within the voids of the zeolitic catalyst. A proton is then transferred directly to methanol to form a reactive arene−methoxonium complex without first returning to the zeolite surface. This proposed mechanism bears resemblance to the concerted reaction pathway described in this paper in that in both pathways, the methylating agent is a methoxonium ion that is not bound to the acid site.

4. CONCLUSIONS

Using equilibrium and free energy metadynamics AIMD simulations at the DFT level of theory, we have studied the methylation of benzene with methanol in H-ZSM-5. With the MTD approach, we were able to explore several alternative pathways, taking into account the flexibility of the zeolite framework and the mobility of the reagents inside the pores, which is not possible with the static approaches that are typically used in heterogeneous catalysis. We have shown that the reaction is complex, involving the formation and cleavage of several hydrogen bonds, and that the reaction pathway can be divided into distinct phases. Different methanol loadings and orientations were investigated. In the reactant state at high methanol loadings, protonated methanol clusters are formed, which are relatively stable and mobile. Because of their mobility, several orientations of the methanol-benzene pair with respect to the zeolite framework are possible in the methylation reaction. In addition, methylation can occur at remote locations relative to the catalytic acid site, which suggests that the exact location of the acid site does not significantly influence the reactivity. Benzene, located in the channel intersection, preferentially orients its planar ring parallel with the channels, mainly with the straight channel. Methylation from a protonated and H-bonded methanol cluster is more highly activated than methylation

dx.doi.org/10.1021/cs400706e | ACS Catal. 2013, 3, 2556−2567

from a single protonated methanol molecule inside the channel intersection. Furthermore, comparison with a pure methanol solvent simulation for the benzene methylation reaction indicates that the main role of the zeolite during the methylation of benzene is to provide the acidic proton and to create a polar environment for the reaction. This can be attributed to the relatively small size of the benzene molecule relative to the ZSM-5 pores, which allows it to more or less freely rotate inside the channel intersection, and to the limited strength of interaction between benzene and the zeolite inner surface, despite the preference for certain orientations. Although the confinement effect of the zeolite on the methylation of benzene appears to be relatively small, greater effects are expected in the methylation of polymethylated benzenes. Finally, comparison of the concerted and stepwise methylation reactions shows that the concerted pathway is only slightly favored over the stepwise mechanism, which involves a framework-bound methoxy intermediate. This suggests that both mechanisms may take place, depending on the reaction conditions.

■ ASSOCIATED CONTENT

Supporting Information

Scheme S1, Figures S1−S8, Tables S1−S5, full Gaussian reference, *XYZ* coordinates of static calculations. This material is available free of charge via the Internet at http://pubs.acs.org.

■ AUTHOR INFORMATION

Corresponding Author

*Phone +32 9 264 65 58. E-mail: veronique.vanspeybroeck@ugent.be.

Author Contributions

‡S.L.C.M. and K.D.W. contributed equally to this work.

Notes

The authors declare no competing financial interest.

■ ACKNOWLEDGMENTS

We are grateful to the Research Foundation−Flanders (FWO), the Research Board of Ghent University, and BELSPO in the frame of IAP P7/05. Funding was also received from the European Research Council under the European Community's Seventh Framework Program [FP7(2007-2013) ERC Grant Agreement No. 240483]. Computational resources and services used in this work were provided by the Stevin Supercomputer Infrastructure of Ghent University.

■ REFERENCES

(1) Hemelsoet, K.; Van der Mynsbrugge, J.; De Wispelaere, K.; Waroquier, M.; Van Speybroeck, V. *ChemPhysChem* **2013**, *14* (8), 1526−1545.

(2) Ilias, S.; Bhan, A. *ACS Catal.* **2013**, *3*, 18−31.

(3) Olsbye, U.; Svelle, S.; Bjørgen, M.; Beato, P.; Janssens, T. V. W.; Joensen, F.; Bordiga, S.; Lillerud, K. P. *Angew.Chem., Int. Ed.* **2012**, *51*, 5810−5831.

(4) Stöcker, M. *Microporous Mesoporous Mater.* **1999**, *29*, 3−48.

(5) Chen, J. Q.; Bozzano, A.; Glover, B.; Fuglerud, T.; Kvisle, S. *Catal. Today* **2005**, *106*, 103−107.

(6) Dahl, I. M.; Kolboe, S. *J. Catal.* **1994**, *149*, 458−464.

(7) Lesthaeghe, D.; Van Speybroeck, V.; Marin, G. B.; Waroquier, M. *Angew. Chem., Int. Ed.* **2006**, *45*, 1714−1719.

(8) Song, W. G.; Marcus, D. M.; Fu, H.; Ehresmann, J. O.; Haw, J. F. *J. Am. Chem. Soc.* **2002**, *124*, 3844−3845.

(9) Bjørgen, M.; Svelle, S.; Joensen, F.; Nerlov, J.; Kolboe, S.; Bonino, F.; Palumbo, L.; Bordiga, S.; Olsbye, U. *J. Catal.* **2007**, *249*, 195−207.

(10) Dahl, I. M.; Kolboe, S. *Catal. Lett.* **1993**, *20*, 329−336.

(11) Dahl, I. M.; Kolboe, S. *J. Catal.* **1996**, *161*, 304−309.

(12) Haw, J. F.; Song, W. G.; Marcus, D. M.; Nicholas, J. B. *Acc. Chem. Res.* **2003**, *36*, 317−326.

(13) Svelle, S.; Joensen, F.; Nerlov, J.; Olsbye, U.; Lillerud, K. P.; Kolboe, S.; Bjørgen, M. *J. Am. Chem. Soc.* **2006**, *128*, 14770−14771.

(14) Corma, A.; Sastre, G.; Viruela, P. M. *J. Mol. Catal. A: Chem.* **1995**, *100*, 75−85.

(15) De Wispelaere, K.; Hemelsoet, K.; Waroquier, M.; Van Speybroeck, V. *J. Catal.* **2013**, *305*, 76−80.

(16) Lesthaeghe, D.; De Sterck, B.; Van Speybroeck, V.; Marin, G. B.; Waroquier, M. *Angew. Chem., Int. Ed.* **2007**, *46*, 1311−1314.

(17) Lesthaeghe, D.; Horre, A.; Waroquier, M.; Marin, G. B.; Van Speybroeck, V. *Chem.—Eur. J.* **2009**, *15*, 10803−10808.

(18) McCann, D. M.; Lesthaeghe, D.; Kletnieks, P. W.; Guenther, D. R.; Hayman, M. J.; Van Speybroeck, V.; Waroquier, M.; Haw, J. F. *Angew. Chem., Int. Ed.* **2008**, *47*, 5179−5182.

(19) Wang, C. M.; Wang, Y. D.; Xie, Z. K.; Liu, Z. P. *J. Phys. Chem. C* **2009**, *113*, 4584−4591.

(20) Hill, I. M.; Al Hashimi, S.; Bhan, A. *J. Catal.* **2012**, *285*, 115−123.

(21) Svelle, S.; Ronning, P. A.; Kolboe, S. *J. Catal.* **2004**, *224*, 115−123.

(22) Svelle, S.; Ronning, P. O.; Olsbye, U.; Kolboe, S. *J. Catal.* **2005**, *234*, 385−400.

(23) Svelle, S.; Visur, M.; Olsbye, U.; Saepurahman; Bjørgen, M. *Top. Catal.* **2011**, *54*, 897−906.

(24) Svelle, S.; Bjørgen, M. *J. Phys. Chem. A* **2010**, *114*, 12548−12554.

(25) Vos, A. M.; Nulens, K. H. L.; De Proft, F.; Schoonheydt, R. A.; Geerlings, P. *J. Phys. Chem. B* **2002**, *106*, 2026−2034.

(26) Svelle, S.; Arstad, B.; Kolboe, S.; Swang, O. *J. Phys. Chem. B* **2003**, *107*, 9281−9289.

(27) Van Speybroeck, V.; Van der Mynsbrugge, J.; Vandichel, M.; Hemelsoet, K.; Lesthaeghe, D.; Ghysels, A.; Marin, G. B.; Waroquier, M. *J. Am. Chem. Soc.* **2011**, *133*, 888−899.

(28) Svelle, S.; Tuma, C.; Rozanska, X.; Kerber, T.; Sauer, J. *J. Am. Chem. Soc.* **2009**, *131*, 816−825.

(29) Van der Mynsbrugge, J.; Visur, M.; Olsbye, U.; Beato, P.; Bjørgen, M.; Van Speybroeck, V.; Svelle, S. *J. Catal.* **2012**, *292*, 201−212.

(30) Chai, J. D.; Head-Gordon, M. *Phys. Chem. Chem. Phys.* **2008**, *10*, 6615−6620.

(31) Zimmermann, N. E. R.; Jakobtorweihen, S.; Beerdsen, E.; Smit, B.; Keil, F. J. *J. Phys. Chem. C* **2007**, *111*, 17370−17381.

(32) Kapko, V.; Dawson, C.; Treacy, M. M. J.; Thorpe, M. F. *Phys. Chem. Chem. Phys.* **2010**, *12*, 8531−8541.

(33) Smit, B.; Maesen, T. L. M. *Chem. Rev.* **2008**, *108*, 4125−4184.

(34) Brennan, J. A.; Lucki, S. J.; Schoennagel, H. J. Catalysts for the conversion of methanol to ethylene plus gasoline; U.S. Patent US 4,480,145, 1984.

(35) Kaeding, W. W. Zeolite catalyst containing oxide of boron or magnesium; U.S. Patent 4,049,573, 1977.

(36) Kaeding, W. W.; Butter, S. A. Conversion of methanol and dimethyl ether; U.S. Patent 3,911,041, 1975.

(37) Brown, S. H.; Shinnar, R.; Weber, W. A. Process for converting methanol to olefins; U.S. Patent 6,613,951, 2003.

(38) Mole, T.; Seddon, D.; Whiteside, J. A. Methanol conversion to hydrocarbons with zeolites and cocatalysts; U.S. Patent 4,499,314, 1985.

(39) Marchi, A. J.; Froment, G. F. *Appl. Catal.* **1991**, *71*, 139−152.

(40) Dehertog, W. J. H.; Froment, G. F. *Appl. Catal.* **1991**, *71*, 153−165.

(41) Song, W.; Fu, H.; Haw, J. F. *J. Am. Chem. Soc.* **2001**, *123*, 4749−4754.

(42) Alwahabi, S. M.; Froment, G. F. *Ind. Eng. Chem. Res.* **2004**, *43*, 5098−5111.

(43) Zheng, A. M.; Han, B.; Li, B. J.; Liu, S. B.; Deng, F. *Chem. Commun.* **2012**, *48*, 6936−6938.

(44) Benco, L.; Bucko, T.; Hafner, J. *J. Catal.* **2011**, *277*, 104−116.

(45) Bucko, T.; Benco, L.; Hafner, J.; Angyan, J. G. *J. Catal.* **2011**, *279*, 220−228.

(46) Benco, L.; Bucko, T.; Hafner, J. *J. Phys. Chem. C* **2009**, *113*, 18807−18816.

(47) Bucko, T.; Benco, L.; Dubay, O.; Dellago, C.; Hafner, J. *J. Chem. Phys.* **2009**, *131*, 11.
(48) Bucko, T.; Benco, L.; Hafner, J.; Angyan, J. G. *J. Catal.* **2007**, *250*, 171−183.
(49) Database of zeolite structures. http://www.iza-structure.org/databases/
(50) VandeVondele, J.; Krack, M.; Mohamed, F.; Parrinello, M.; Chassaing, T.; Hutter, J. R. *Comput. Phys. Commun.* **2005**, *167*, 103−128.
(51) Lippert, G.; Hutter, J.; Parrinello, M. *Mol. Phys.* **1997**, *92*, 477−487.
(52) Lippert, G.; Hutter, J.; Parrinello, M. *Theor. Chem. Acc.* **1999**, *103*, 124−140.
(53) Yang, K.; Zheng, J. J.; Zhao, Y.; Truhlar, D. G. *J. Chem. Phys.* **2010**, *132*, 10.
(54) Goedecker, S.; Teter, M.; Hutter, J. *Phys. Rev. B* **1996**, *54*, 1703−1710.
(55) Grimme, S.; Antony, J.; Ehrlich, S.; Krieg, H. *J. Chem. Phys.* **2010**, *132*.
(56) Laio, A.; Parrinello, M. *Proc. Natl. Acad. Sci. U.S.A.* **2002**, *99*, 12562−12566.
(57) Laio, A.; Gervasio, F. L. *Rep. Prog. Phys.* **2008**, *71*, 22.
(58) Bussi, G.; Laio, A.; Parrinello, M. *Phys. Rev. Lett.* **2006**, *96*, 090601.
(59) Frisch, M. J.; Trucks, G. W.; Schlegel, H. B.; Scuseria, G. E.; Robb, M. A.; Cheeseman, J. R.; Scalmani, G.; Barone, V.; Mennucci, B.; Petersson, G. A.; Nakatsuji, H.; Caricato, M.; Li, X.; Hratchian, H. P.; Izmaylov, A. F.; Bloino, J.; Zheng, G.; Sonnenberg, J. L.; Hada, M.; Ehara, M.; Toyota, K.; Fukuda, R.; Hasegawa, J.; Ishida, M.; Nakajima, T.; Honda, Y.; Kitao, O.; Nakai, H.; Vreven, T.; Montgomery, J. A., Jr.; Peralta, J. E.; Ogliaro, F.; Bearpark, M.; Heyd, J. J.; Brothers, E.; Kudin, K. N.; Staroverov, V. N.; Kobayashi, R.; Normand, J.; Raghavachari, K.; Rendell, A.; Burant, J. C.; Iyengar, S. S.; Tomasi, J.; Cossi, M.; Rega, N.; Millam, N. J.; Klene, M.; Knox, J. E.; Cross, J. B.; Bakken, V.; Adamo, C.; Jaramillo, J.; Gomperts, R.; Stratmann, R. E.; Yazyev, O.; Austin, A. J.; Cammi, R.; Pomelli, C.; Ochterski, J. W.; Martin, R. L.; Morokuma, K.; Zakrzewski, V. G.; Voth, G. A.; Salvador, P.; Dannenberg, J. J.; Dapprich, S.; Daniels, A. D.; Farkas, Ö.; Foresman, J. B.; Ortiz, J. V.; Cioslowski, J.; Fox, D. J. *Gaussian 09, Revision B.01*; Gaussian, Inc.: Wallingford, CT, 2009.
(60) Ghysels, A.; Verstraelen, T.; Hemelsoet, K.; Waroquier, M.; Van Speybroeck, V. *J. Chem. Inf. Model.* **2010**, *50*, 1736−1750.
(61) CMM Code. http://molmod.ugent.be/software.
(62) Catak, S.; D'Hooghe, M.; Verstraelen, T.; Hemelsoet, K.; Van Nieuwenhove, A.; Ha, H. J.; Waroquier, M.; De Kimpe, N.; Van Speybroeck, V. *J. Org. Chem.* **2010**, *75*, 4530−4541.
(63) Ivanova, I. I.; Kolyagin, Y. G. *Chem. Soc. Rev.* **2010**, *39*, 5018−5050.
(64) Hunger, B.; Matysik, S.; Heuchel, M.; Einicke, W.-D. *Langmuir* **1997**, *13*, 6249−6254.
(65) Hunger, M.; Horvath, T. *J. Am. Chem. Soc.* **1996**, *118*, 12302−12308.
(66) Harris, K. D. M.; Xu, M. C.; Thomas, J. M. *Philos. Mag.* **2009**, *89*, 3001−3012.
(67) Termath, V.; Haase, F.; Sauer, J.; Hutter, J.; Parrinello, M. *J. Am. Chem. Soc.* **1998**, *120*, 8512−8516.
(68) Tuma, C.; Kerber, T.; Sauer, J. *Angew. Chem., Int. Ed.* **2010**, *49*, 4678−4680.
(69) Alberti, A.; Martucci, A. *J. Phys. Chem. C* **2010**, *114*, 7767−7773.
(70) Grimsrud, E. P.; Kebarle, P. *J. Am. Chem. Soc.* **1973**, *95*, 7939−7943.
(71) Chang, H.-C.; Jiang, J.-C.; Lin, S. H.; Lee, Y. T.; Chang, H.-C. *J. Phys. Chem A* **1999**, *103*, 2941−2944.
(72) Fifen, J. J.; Nsangou, M.; Dhaouadi, Z.; Motapon, O.; Jaidane, N.-E. *J. Chem. Theory Comp.* **2013**, *9*, 1173−1181.
(73) Knight, C.; Voth, G. A. *Acc. Chem. Res.* **2011**, *45*, 101−109.
(74) Bjørgen, M.; Joensen, F.; Lillerud, K.-P.; Olsbye, U.; Svelle, S. *Catal. Today* **2009**, *142*, 90−97.
(75) Weckhuysen, B. M. *Chem. Commun.* **2002**, 97−110.
(76) Haw, J. F. *In Situ Spectroscopy in Heterogeneous Catalysis*; Wiley-VCH Verlag GmbH & Co. KGaA: Weinheim, FRG, 2004.
(77) Song, W. G.; Nicholas, J. B.; Sassi, A.; Haw, J. F. *Catal. Lett.* **2002**, *81*, 49−53.
(78) Wang, W.; Buchholz, A.; Seiler, M.; Hunger, M. *J. Am. Chem. Soc.* **2003**, *125*, 15260−15267.
(79) Wang, W.; Hunger, M. *Acc. Chem. Res.* **2008**, *41*, 895−904.
(80) Ivanova, I. I.; Corma, A. *J. Phys. Chem. B* **1997**, *101*, 547−551.
(81) Saepurahman; Visur, M.; Olsbye, U.; Bjørgen, M.; Svelle, S. *Top. Catal.* **2011**, *54*, 1293−1301.
(82) Svelle, S.; Kolboe, S.; Swang, O.; Olsbye, U. *J. Phys. Chem. B* **2005**, *109*, 12874−12878.
(83) Maihom, T.; Boekfa, B.; Sirijaraensre, J.; Nanok, T.; Probst, M.; Limtrakul, J. *J. Phys. Chem. C* **2009**, *113*, 6654−6662.